International Journal of Pharmaceutics: X 9 (2025) 100322

Contents lists available at ScienceDirect

International Journal of Pharmaceutics: X

journal homepage: www.sciencedirect.com/journal/international-journal-of-pharmaceutics-x

Exploring the potential of antifungal-loaded proniosomes to consolidate corneal permeation in fungal keratitis: A comprehensive investigation from laboratory characterization to microbiological evaluation

Sadek Ahmed [a], Michael M. Farag [a,*], Heba Attia [b], Bander Balkhi [c], Islam M. Adel [a], Asmaa Ashraf Nemr [a]

[a] Department of Pharmaceutics and Industrial Pharmacy, Faculty of Pharmacy, Cairo University, Cairo 11562, Egypt
[b] Department of Microbiology and Immunology, Faculty of Pharmacy, Cairo University, Cairo 11562, Egypt
[c] Department of Clinical Pharmacy, College of Pharmacy, King Saud University, Riyadh, Saudi Arabia

ARTICLE INFO

Keywords:
Terconazole
Proniosomes
Fungal keratitis
Biofilm inhibition
Ex-vivo permeation

ABSTRACT

This work aimed to prepare Terconazole loaded proniosomes (TCZ-PNS) utilizing modified coacervation technique for the management of fungal keratitis. Terconazole (TCZ) is a potent antifungal with poor aqueous solubility posing intricacies in its incorporation in ocular formulations. A 2^3 factorial design was adopted to probe independent formulation variables including A: Lecithin: cholesterol ratio, B: Surfactant: cholesterol ratio and C: Span® 80 contribution (% of total SAA). The formulae, generated by the design, were prepared and scrutinized regarding entrapment efficiency (%EE), particle size (PS), polydispersity index (PDI) and zeta potential (ZP). Numerical desirability algorithms selected an optimum TCZ-PNS which boasted plausible %EE (89.51 % ± 0.94 %), nanoscale vesicles consistent with TEM measurements (247.9 ± 0.42 nm), a sufficiently high ZP (−43.42 ± 0.85 mV), and an in-vitro biphasic release profile that remained stable even after Gamma irradiation and short-term storage. The transcorneal ex-vivo permeation of TCZ-PNS was higher than that of TCZ suspension (≈ 2-fold). The formulation was further evaluated for pH, corneal hydration threshold, and histopathological safety, confirming its suitability for ocular application. Confocal laser microscopy revealed substantial corneal uptake (approximately twice as deep as of TCZ suspension). Additionally, microbiological assessments of the optimal TCZ-PNS compared to TCZ suspension demonstrated an inhibition zone nearly 50 % larger, a significantly lower MIC and MFC (64-fold reduction), and enhanced biofilm inhibition activity across most tested concentrations. These findings suggest that TCZ-PNS could be a propitious treatment choice to deeply deliver antifungal therapy for the eradication of deeply rooted and inaccessible fungal keratitis.

1. Introduction

Fungal keratitis is a detrimental corneal infection and an eminent culprit behind corneal inflammation and ulceration with substantial ramifications on the eyesight, it is ranked as a major cause of corneal blindness which is the second common form of blindness (Awad et al., 2024; Sharma et al., 2022). Fungal keratitis thrives in regions characterized with warm and damp climate, where farming is the predominant occupation and commonly escorted with poor hygiene predisposing individuals to fungal eye infections representing more than half of ocular ailments (Bongomin et al., 2017; Leck et al., 2002). Notably, even among third-world countries, fungal keratitis is more prevalent among financially compromised individuals who wear contact lens (Brown et al., 2021).

Recent judicious estimates aligned with previous forecasts, made twenty years ago, emphasized startling escalations of new cases estimated to reach approximately 1.5 million/year (Brown et al., 2021; Whitcher et al., 2001). The underlying etiology behind such infections includes chronic corticosteroids uptake, the incautious use of contact lenses without proper sanitary precautions, superficial corneal diseases, ophthalmic surgeries, and immunocompromised conditions (Qiao et al., 2020).

Fungal keratitis can be treated using different antifungal agents classified based on their chemical structure into polyenes, azoles,

* Corresponding author at: Department of Pharmaceutics and Industrial pharmacy, Faculty of Pharmacy, Cairo University, Kasr El-Aini Street, Cairo 11562, Egypt.
E-mail address: michael.farag@pharma.cu.edu.eg (M.M. Farag).

https://doi.org/10.1016/j.ijpx.2025.100322
Received 4 January 2025; Received in revised form 21 February 2025; Accepted 22 February 2025
Available online 24 February 2025

echinocandins, and allylamines (Ahmed et al., 2024a; Al-Badriyeh et al., 2010). Azoles are synthetic antifungals which tend to inhibit sterol demethylase enzyme responsible for converting lanosterol into ergosterol thwarting fungal cell membrane formation. Thus, causing increased fungal membrane permeability, accumulation of noxious methyl sterols, hindered mycotic cell division and eventually fungal cell death (El-Emam et al., 2020; Gavarkar et al., 2013).

Terconazole (TCZ), is a potent antifungal, belonging to the azoles and proved its worth against filamentous fungi and yeasts. The poor aqueous solubility of TCZ (pKa = 8, log $P = 5.37$) poses intricacies in its incorporation in ophthalmic preparations such as poor solubility, irritation and stability issues (Mirza et al., 2017; Zaghloul et al., 2022b). Intriguingly, a review of literature revealed numerous endeavors to utilize terconazole for ocular delivery, including the development of PLGA microparticles (Zaghloul et al., 2022b), cationic polymeric nanoparticles (Mohsen, 2022), bilosomes (Abdelbary et al., 2016), integrated self-nanoemulsifying/bilosome system (Yousry et al., 2020) and silica/chitosan nanoparticles (Zaghloul et al., 2022a).

Eye drops are preferred for the ocular delivery of antifungal agents for the eradication of fungal keratitis (Al-Badriyeh et al., 2009). The ease of instillation, prompt onset of action, patient's compliance, cost effectiveness, lack of invasiveness, and reduced systemic side effects account for this preference (Davies, 2000). Nevertheless, conventional eye drops have short residence time and limited bioavailability not exceeding 5 % (Casey-Power et al., 2022) caused by involuntarily blinking, pre-corneal metabolism and cornea's epithelium's tight junctions (Ding et al., 2018; Gaudana et al., 2010; Mannermaa et al., 2006). Moreover, up to 10-fold reduction of ocular drug concentration is speculated due to tear film dilution induced by eye hydration through lacrimation (Casey-Power et al., 2022).

Proniosomes are revolutionary modulated paragons of traditional niosomes that can be prepared either as flowable powder or as liquid crystal pseudoplastic gel. Proniosomes are basically composed of hydrophilic carriers coated with non-ionic surfactants. Upon reconstitution with water at temperature exceeding the surfactant's transition temperature, they transform into uniformly dispersed niosomes counterpart (Abdelbary et al., 2017). Proniosomes offer myriads of benefits relative to their ancestor niosomes, boasting a more homogenous size and better stability profile. They circumvent physical challenges such as drug hydrolysis, pre-mature leakage, aggregation, sedimentation, and fusion during storage. Additionally, they are versatile enough to encapsulate drugs with varying solubility profiles (Mosallam et al., 2022). Literature review accentuated the pivotal role of proniosomes in augmenting the bioavailability of numerous drugs and specially antifungal agents including: itraconazole (Ismail and Khattab, 2018), ketoconazole (Abdelbary et al., 2017), voriconazole (El-Emam et al., 2020), clotrimazole (Kondawar et al., 2011) and ciclopirox (Mahajan et al., 2021).

In the notion of the aforementioned traits, this study aimed to prepare Terconazole loaded proniosomes (TCZ-PNS) to enhance the drug's transcorneal absorption. A 2^3 full factorial design was adopted to evaluate the significance of the scrutinized independent factors namely, lecithin: cholesterol ratio, surfactant: cholesterol ratio and Span® 80 contribution (% of total SAA) on the targeted dependent responses encompassing %EE, PS (nm), PDI and ZP (mV). The optimum formulation, selected based on numerical optimization, underwent a comprehensive assessment entailing in-vitro release kinetic analysis, stability following short-term storage, effect of sterilization by gamma irradiation, and ex-vivo corneal penetration, benchmarked against TCZ suspension. Additionally, the optimum formulation's safety profile was meticulously examined using histopathological analysis, assessment of corneal hydration, and pH measurement to confirm its safety for ocular application. In-vivo efficacy was further appraised by measuring corneal uptake using confocal laser microscopy and conducting a series of microbiological evaluations.

2. Materials and methods

2.1. Materials

Terconazole (TCZ) was kindly gifted by Marcyrl Pharmaceutical Industries, Egypt. Lecithin, Cholesterol, Brij® 92 (polyoxyethylene 2 oleylether) and dialysis membrane (Mwt cutoff 14 KDa) were procured from Sigma-Aldrich® (St. Louis, MO, USA). Methanol, acetone, Span® 80 (sorbitan monooleate), potassium dihydrogen phosphate, disodium hydrogen phosphate, sodium chloride and potassium chloride were procured from El-Nasr Pharmaceutical Chemicals Co. (Cairo, Egypt). The remaining reagents were of analytical grade.

2.2. Animals

The study strictly followed the laboratory animal care guidelines published by the US National Institute of Health (Council et al., 2011). Adult rabbits (male, albino, 2.26 ± 0.27 kg) were individually caged with an equally alternating light/dark cycle at room temperature (25 ± 2 °C). The rabbits were provided with tap water and standard commercial food throughout the study. Prior to the start of the study, all rabbits underwent ocular inspection, and any rabbit displayed ocular inflammatory signs was excluded. The Ethics Committee, Faculty of Pharmacy, Cairo University has ratified this research, approval no. (PI 3504). This study complies with the "ARRIVE guidelines for reporting *in-vivo* experiments". Also, we have abided by the guidelines described in the "Guide for Care and Use of Laboratory Animals", which were published by the US National Institute of Health (No. 85–23, revised in 2011).

2.3. Methods

2.3.1. Experimental design

A 2^3 factorial design was adopted to statistically optimize three independent variables in the formulation of terconazole-loaded proniosomes (TCZ-PNS) including, A: Lecithin: cholesterol ratio, B: Surfactant: cholesterol ratio and C: Span® 80 contribution (% of total SAA). Each factor was tested at 2 different levels, based on preliminary investigations, resulting in eight formulae (F1-F8) suggested by Design Expert® software (Version 12, Stat-Ease Inc., MN, USA). The characterization and further selection of the optimum formula was based on measuring %EE PS (nm), PDI and ZP (mV) and setting desirability restraints as summarized in Table (1) (Farag et al., 2023a).

2.3.2. Preparation of Terconazole-loaded proniosomes (TCZ-PNS)

Terconazole-loaded proniosomes (TCZ-PNS) were developed adopting a modified coacervation technique (Younes et al., 2024). The exact composition of the developed formulae is summarized in table (2). Briefly, accurately weighed cholesterol (50 mg), surfactant mixture (Span® 80 and Brij® 92), lecithin, and TCZ (10 mg) were dispersed in 2 mL of a methanol: acetone mixture (1:1 *v*/v) placed in vial. Then, the sealed vial was placed in an ultrasonic bath sonicator (Model SH 150–41, MTI Corporation, Richmond, CA) for 0.5 h at 60 °C till the formation of clear organic phase. Subsequently, 3 drops of preheated (60 °C) phosphate buffer saline (PBS, pH 7.4) were added dropwise into the prepared organic phase. The mixture was sonicated for another 25 min until it became clear. Afterward, the mixture was left to cool at room temperature overnight, resulting in the formation of translucent dispersion.

2.3.3. In-vitro characterization of TCZ-PNS

Each formulation was first heated at 60 °C for 1 min, then reconstituted with PBS, followed by sonication at 60 °C for another minute. The mixture was then vortexed for 5 min, resulting in 10 mL of TCZ-loaded niosomes (TCZ-NS), which were subsequently subjected to the following characterizations.

2.3.3.1. Determination of the entrapment efficiency (%EE). The %EE of the reconstituted TCZ-NS was determined adopting indirect method (Abdelbary and AbouGhaly, 2015). An aliquot (1 mL) of niosomal dispersion was centrifuged at 21000 rpm for 1 h at 4 °C (Sigma 3–30 KS cooling ultracentrifuge, Sigma Laborzentrifugen GmbH, Osterode am Harz, Germany). Subsequently, the supernatant containing unentrapped TCZ was diluted (1:10) with methanol and measured spectrophotometrically at 254 nm against plain niosomal dispersion as blank (Shimadzu UV-1601 PC spectrophotometer, Kyoto, Japan) (Abdelbary et al., 2016). The results of %EE of three different experiments were expressed as mean ± SD. The %EE was computed by the following equation (Ahmed et al., 2024b):

$$\%EE = \frac{Total\ theoretical\ TCZ - unentrapped\ TCZ}{Total\ theoretical\ TCZ} \times 100$$

2.3.3.2. Determination of particle size (PS), polydispersity index (PDI) and zeta potential (ZP). The PS, PDI and ZP of the reconstituted TCZ-NS were measured using Zetasizer Nano ZS (Malvern instruments; Worcestershire, UK). Briefly, an aliquot (100 µL) of niosomal dispersion was added to 10 mL double distilled water to achieve suitable scattering intensity (El Taweel et al., 2023). Experiments were done in triplicates at room temperature (25 °C ± 2 °C).

2.3.4. Statistical optimization and validation

The numerical desirability algorithms integrated within the Design Expert® software were employed to statistically optimize the scrutinized independent variables. This optimization was guided by the restraints imposed on the measured responses, as provided in Table 1. To fairly assess the accuracy of the selected model, the proposed optimum formula was prepared and re-evaluated regarding targeted responses. Subsequently, statistical analysis using one-way ANOVA was used to test the significance of the difference ($\alpha = 0.05$) existed between the actual and prognosticated mean values of the measured responses (Habib et al., 2018; Nemr et al., 2024).

2.3.5. Characterization of the optimum TCZ-PNS

2.3.5.1. Fourier-transform infra-red spectroscopy (FTIR). The optimum TCZ-PNS was frozen at −2 °C, then freeze dried for 24 h at (7×10^2 mbar, −45 °C) using Novalyphe lyophilizer (Novalyphe-NL 500; Savant Instruments Corp., Hicksville, NY). Then, samples of TCZ, Cholesterol, Lecithin and lyophilized optimum TCZ-PNS were analyzed using an FTIR spectrophotometer (Bruker model 22, Coventry, UK). Briefly, each ingredient was accurately weighed (5 mg) and mixed with dry potassium bromide using geometric dilution technique prior to compression into a disc. Subsequently, the discs were scanned at room temperature (25 °C ± 2 °C) over 4000–500 cm^{-1} (Younes et al., 2024).

2.3.5.2. Transmission electron microscopy (TEM). The shape and size of the optimum TCZ-PNS vesicles were determined using TEM (Joel JEM 1400, Tokyo, Japan). The proniosomal dispersion was diluted (1: 20) with double distilled water and then filtered to get rid of any clumps. Subsequently, 2 drops of the dispersion were stained using phosphotungstic acid (1 %). Consequently, a copper grid coated with a carbon layer was dipped in the sample and air-dried to form a thin film before examination (Farag et al., 2023b).

Table 1
The scrutinized independent variables of the 2^3 factorial design and applied desirability constraints.

Factors (independent variable)	Level	
	-1	1
A: Lecithin: Cholesterol	3	6
B: SAA[a]: Cholesterol	1.5	3
C: Span® 80 contribution (% of total SAA)	30	60
Response (dependent variable)	**Desirability constraints**	
Y1: Entrapment efficiency (%)	Maximize	
Y2: Particle size (nm)	In range	
Y3: Polydispersity index	In range	
Y4: Zeta potential (mV)	Maximize (as absolute value)	

SAA[a], Surfactant.

2.3.5.3. Comparative in-vitro release study. A dialysis bag was used for the determination of the in-vitro release profiles of the optimum TCZ-PNS versus TCZ suspension (1 mg/mL) (Weng et al., 2020). Briefly, the donor compartment contained an accurate volume corresponding to 2 mg of TCZ of both TCZ-PNS dispersion and TCZ suspension, were loaded into Spectra Por® dialysis bag (12,000–14,000 Da cutoff), which was previously soaked overnight. Subsequently, the dialysis bag was sealed and immersed in corked glass bottles filled with 50 mL PBS (pH 7.4) containing 10 % methanol as the receptor compartment. The bottles were fixed in a water bath shaker (Unimax, IKA, Staufen, Germany) operated at 60 strokes per minute and adjusted at 37 ± 1 °C (Shahab et al., 2020). Aliquots (3 mL) were taken from the receptor compartment at fixed intervals (0, 0.5, 1, 2, 4, 6, 8 h) and to keep sink condition, the medium was replenished with an equal volume of release medium. Consequently, the determination of the percentage TCZ released at each time point was carried out by analyzing samples spectrophotometrically at 254 nm. Release results were expressed as the average values of three independent experiments.

The in-vitro release profiles of the optimum TCZ-PNS and TCZ suspension were kinetically evaluated by substituting in the equations of zero-order, first-order, and Higuchi diffusion models. The regression coefficient (R^2) for each model was then determined, with the model exhibiting the highest regression coefficient being selected as the representative model of the release pattern for the optimum formula (Farag et al., 2022; Tawfik et al., 2023).

2.3.5.4. Corneal ex-vivo permeation study. Adult male albino rabbits were anesthetized by ketamine (200 mg/kg, IM) and xylazine (20 mg/kg, IM) followed by euthanasia by decapitation (Eldeeb et al., 2019; Sayed et al., 2020). Subsequently, the eyeballs were surgically removed, and careful dissection of the corneas from the globes was performed. Prior to mounting, dissected corneas were thoroughly washed with saline to avoid the compromise of corneal membrane's integrity by ensuring the absence of folds or wrinkles.

Ex-vivo permeation was promptly conducted in Franz diffusion cell (Hanson Research in Chatsworth, USA) following the dissection of corneas (Dai et al., 2013). Accurate volumes of the optimum TCZ-PNS or TCZ suspension (1 mg/mL) equivalent to 2 mg TCZ represented the donor compartment (Farag et al., 2023a; Nemr et al., 2022). Simultaneously, 25 mL of fresh simulated tear fluid (37 ± 0.5 °C, pH 7.4) were stirred in a magnetic stirrer (50 rpm) as the receptor compartment. Dissected cornea secured in a plastic membrane was mounted between both compartments with constant surface area for diffusion (0.5 cm^2). At fixed intervals (0, 1, 2, 4, 6, 8, 10 h), samples (2 mL) were taken and immediately replenished with fresh media to preserve the sink condition in the receptor compartment. After that, samples were filtered using nylon filter (0.22 µm) before spectrophotometric analysis at 254 nm against a blank medium in which cornea was mounted without any applied formula (ElMeshad and Mohsen, 2016; Kouchak et al., 2019).

The ex-vivo permeation profile was illustrated by plotting cumulative drug permeated (mg/cm^2) versus time (h). Also, the maximum flux (J_{max}) determined at 10 h alongside the calculation of the enhancement ratio (ER) using these equations (Younes et al., 2018):

$$Jmax = \frac{Amount\ of\ drug\ permeated}{Time \times area\ of\ membrane}$$

$$ER = \frac{Jmax\ of\ TCZ - PNS}{Jmax\ of\ TCZ\ suspension\ (control)}$$

2.3.5.5. Corneal hydration threshold (%HT). The test was carried out to evaluate potential tissue damage resulted from improper handling or applied formulation during the permeability study (Aka and Haji, 2015; Liu et al., 2005). Promptly, after completing the previous ex-vivo permeation experiment, each cornea was carefully removed and washed with saline to eliminate any superficial debris. The corneas were then blotted with filter paper to absorb extra moisture before being initially weighed (Wi). Subsequently, they were dried at 50 °C for 24 h in the oven and weighed again (Wf). The percentage corneal hydration threshold (%HT) was calculated using this equation (Ahmed et al., 2022b; Moustafa et al., 2017):

$$\%HT = \left[1 - \left(\frac{Wi}{Wf}\right)\right] \times 100$$

2.3.5.6. Effect of short-term storage and Gamma irradiation. In a refrigerator (5 ± 3 °C), a sealed amber colored vial containing the optimum formula was stored for three months. Simultaneously, another freshly prepared optimum formula was terminally sterilized by gamma irradiation at 10 kGy dose obtained from a ^{60}Co irradiation source. By the end of storage period and gamma sterilization, the relevant parameters, including %EE, PS, and ZP, were re-evaluated. To determine any statistically significant changes during sterilization and storage, a one-way ANOVA was performed using SPSS software version 26.0 (SPSS Inc., Chicago, IL, USA) (Emad Eldeeb et al., 2019). Additionally, the in-vitro release profile was compared before and after storage and sterilization through the calculation of similarity factor using the specified equation (Nemr et al., 2021; Sayed et al., 2021) to detect possible changes in release profile:

$$f_2 = 50.log\left\{\left[1 + \left(\frac{1}{n}\right)\sum_{t=1}^{n}(R_t - T_t)^2\right]^{-0.5}.100\right.$$

Where Rt and Tt stands for the %TCZ released before and after the storage period or gamma sterilization respectively. To confirm the similarity between the release profiles, a value greater than 50 is required.

2.3.6. Safety evaluation

2.3.6.1. Histopathological evaluation. Albino rabbits ($n = 6$, males) were used in the histopathological evaluation to detect any abnormalities in the rabbits' eyes following the instillation of the optimum TCZ-PNS dispersion. A physical examination for all rabbits was performed pre-study to exclude those displaying any signs of ocular inflammation/redness. For one week, one drop of either the optimum TCZ-PNS dispersion or saline (negative control) was instilled every 8 h in the rabbits' right and left eyeballs' cul-de-sac respectively. Post-study, the rabbits' eyeballs were surgically removed following euthanasia, thoroughly cleaned with PBS (pH 7.4), and stored till further analysis in jars containing 10 % formalin saline solution.

Prior to analysis, dissected corneal membranes were dehydrated using serial alcohol dilutions, dehydrated samples were soaked in xylene and mounted in paraffin blocks at 56 °C for one day. A rotary microtome (Leica Microsystems SM2400, Cambridge, UK) was used to cut tissue sections (thickness = 4 μm). After that, stained sections with hematoxylin and eosin were affixed to glass slides to be visualized under light microscope (Leica Imaging Systems Ltd., Cambridge, England) (Abdellatif et al., 2022).

2.3.6.2. Formulation's pH measurement. Measuring formulation's pH is essential for evaluating the compatibility of ocular formulations (Sayed et al., 2021). The optimum pH of ocular formulations should be ranging from 3.5 to 8.5 otherwise applied formulations are susceptible to drainage upon excessive lacrimation induced by ocular irritation (Alhakamy et al., 2022). The measured pH of the optimum TCZ-PNS formula was presented as mean ± SD ($n = 3$) using pH meter (Jenway model-3505, Bibby Scientific Ltd., UK).

2.3.7. In-vivo permeation and microbiological evaluation

2.3.7.1. Confocal laser microscopy (CLM). The penetration depth of the optimum TCZ-PNS was visualized using Confocal Laser microscopy (LSM 710; Carl Zeiss, Jena, Germany) by substituting TCZ by Rhodamine B (RhB 0.1 % *w*/w). Briefly, an aliquot (0.1 mL) of RhB-PNS was instilled to the right eye of male albino rabbits. Simultaneously, an aliquot (0.1 mL) of RhB-solution was instilled in the left eye as negative control. The rabbits were euthanized after 6 h, their corneas were meticulously dissected and washed from debris with saline and stored in artificial tear fluid till imaging. Argon and Helium-neon lasers were used to induce excitation (485 and 595 nm respectively) to measure RhB fluorescence. LSM 4.2 software (Carl Zeiss Microimaging, Jena, Germany) was utilized to handle confocal images (Younes et al., 2018).

2.3.7.2. Kirby–Bauer disk-diffusion susceptibility test. The antifungal activity of TCZ-PNS was assessed and compared to the activity of TCZ using the standard Kirby–Bauer disk diffusion method, following the guidelines established by the Clinical and Laboratory Standards Institute (CLSI, 2018a). Yeast inoculum was prepared by suspending 2–5 distinct *Candida albicans* ATCC 60193 colonies grown on Sabouraud Dextrose Agar (SDA), in sterile saline and the suspension's turbidity was adjusted to match the 0.5 McFarland standard. Muller-Hinton Agar plates - enriched with glucose and methylene blue- were then surface-inoculated with the adjusted yeast suspension. Filter paper discs (sterile and impregnated with 10 μL of either the TCZ suspension or the optimum TCZ-PNS) were allowed to dry and then dispensed on the yeast-inoculated SDA plates. The plates were incubated at 28 ± 2 °C for 48 h, after which the diameters of the inhibition zones were measured and recorded. The experiment was conducted three independent times.

2.3.7.3. Minimum inhibitory concentration (MIC) determination. Minimum inhibitory concentration was determined by the broth microdilution technique in accordance with the Clinical and Laboratory Standards Institute guidelines (CLSI, 2018b). Both TCZ suspension and the optimum TCZ-PNS were prepared over a concentration range of 62.5–0.061 μg/mL by the two-fold serial dilution technique, in a total volume of 150 μL double strength Sabouraud Dextrose Broth (SDB) and dispensed into U-shaped bottom, sterile 96-well plates. Subsequently, 15 μL of *Candida albicans* standard strain (ATCC 60193) suspension (yeast inoculum size of 10^5–10^6 CFU/mL) was dispensed to each well. Negative controls (to verify media sterility) and positive controls (to confirm yeast growth) were carried out.

The microtitre plates were incubated at 28 ± 2 °C for 24 h. The microtitre plates were then examined both visually and by recording the turbidity in each well. The absorbance was measured at a wavelength of 600 nm in a 96-well plate reader. The MIC was determined as the lowest concentration that completely inhibited visible growth. The test was performed in biological and technical triplicates.

2.3.7.4. Minimum fungicidal concentration (MFC). For both preparations (TCZ suspension and optimum TCZ-PNS formula), the MFC for both the TCZ suspension and the optimized TCZ-PNS formulation was assessed using the broth microdilution method in accordance with Clinical and Laboratory Standards Institute guidelines(CLSI, 2018b). In brief, two-fold serial dilutions of each preparation were combined with 15 μL of 10^5–10^6 CFU/mL yeast suspension and incubated in 96-well plates at 28 ± 2 °C for 48 h. Then, 10 μL of the mixture from each well, up to the MIC concentration, was spotted onto the surface of Sabouraud Dextrose Agar (SDA) plates.

The plates were then incubated at 28 ± 2 °C for 48 h. The MFC was

expressed as the lowest concentration at which no visible yeast growth was observed. The experiment was conducted in both biological and technical triplicates.

2.3.7.5. Biofilm inhibitory effect of the optimized TCZ-PNS by crystal violet technique. The effect exerted by the TCZ suspension and the optimized TCZ-PNS on biofilm formation by the *Candida albicans* standard strain was determined using previously described methods(Haney et al., 2021; O'Toole, 2011). Briefly, equal volumes of a yeast suspension (10^8 CFU/mL in SDB) and either the TCZ suspension or the optimized TCZ-PNS were loaded in sterile, flat-bottom, non-pyrogenic polystyrene 96-well culture plates. Each well had a total volume of 100 µL, with final drug concentrations corresponding to $^1/_8$, ¼, ½, 1, 2, and 4 X (X is the calculated drug MIC). The plates were then statically incubated at 28 ± 2 °C for 48 h. Negative, positive and color controls were conducted.

After incubation, the optical density (OD_{600}) of the yeast culture was measured using an automated spectrophotometric plate reader (Biotek, Synergy 2, USA). To quantify the biofilm formation, the supernatants were gently removed, and the wells were rinsed twice with sterile saline. The plates were then left to dry thoroughly. The dried formed biofilm was 25 µL of 0.5 % (*w/v*) crystal violet for 30 min at room temperature. After the 30 min incubation, the wells were washed three times with sterile distilled water and dried thoroughly. The crystal violet in the stained biofilm was solubilized by adding 150 µL of 95 % (w/v) ethanol and incubating with shaking at 110 rpm for 15 min. At the end of the experiment, the absorbance of the solubilized crystal violet (OD_{570}) was measured using the same plate reader and normalized against the OD_{600} of the planktonic cultures. The experiment was done in technical triplicates and repeated three independent times. Results were expressed as biofilm inhibition percentage which was calculated using the following equation:

$$Biofilm\ inhibition\% = \frac{OD\ Control - OD\ Test}{OD\ Control} \times 100$$

3. Results and discussion

TCZ-PNS were prepared by modified coacervation technique adopting a 2^3 factorial design generating eight formulae which were scrutinized regarding their %EE, PS, PDI and ZP to select an optimum TCZ-PNS for further in vitro characterization and microbiological evaluation.

3.1. In-vitro characterization of TCZ-PNS

3.1.1. Statistical analysis of %EE

Plausible entrapment efficiency is pivotal for ophthalmic formulations to endow revamped corneal absorption for the laded drug (Abdelbary et al., 2016). TCZ-PNS displayed a high %EE oscillating between 71.51 % ± 1.24 % and 89.51 % ± 0.94 % as summarized in Table 2. ANOVA analysis showed that A: Lecithin: Cholesterol, B: SAA: Cholesterol and C: Span® 80 contribution (% of total SAA) exhibited significant effect on %EE as shown in Table 3.

Table 3
Summary of regression coefficients, adequate precision and significant factors of model responses.

Response	R^2	Adjusted R^2	Predicted R^2	Adequate precision	Significant factors
Y_1: EE[a] (%)	0.9934	0.9885	0.9736	36.456	A, B, C
Y_2: PS[b] (nm)	0.9789	0.9630	0.9155	19.068	A, B
Y_3: PDI[c]	0.9144	0.8502	0.6577	10.762	A, C
Y_4: ZP[d] (mV)	0.8388	0.7179	0.3553	6.831	A, B

EE[a], entrapment efficiency; PS[b], particle size; PDI[c], poly dispersity index; ZP[d], zeta potential.

Lecithin: Cholesterol ratio exhibited a significant positive impact ($P < 0.0001$) on %EE as depicted in Fig. 1A, showing that increasing Lecithin: Cholesterol ratio from 3:1 to 6:1 displayed higher %EE. This could be possibly due to Lecithin's high phase transition temperature (*Tc*) resulting in reduced membrane permeability thereby preventing leakage of laded cargo and preserving drug's entrapment. Similar findings were observed by Abdelbary et al. (2017), Eldeeb et al. (2019) and Sayed et al. (2020).

The positive impact of SAA: Cholesterol on %EE ($P = 0.007$) is illustrated in Fig. 1A, the increase of SAA: Cholesterol ratio from 1.5: 1 to 3: 1 resulted in higher %EE, it is ratified through reviewing literatures lipophilic drugs such as TCZ (log $P = 5.37$) displayed high %EE in presence of lipophilic SAA (Bnyan et al., 2018; Mahale et al., 2012; Taymouri and Varshosaz, 2016). Considering that both Span®80 and Brij® 92 are lipophilic SAA with closer HLB to TCZ (HLB ≈ 4.3 and 5 respectively (El-Emam et al., 2020; Sayed et al., 2020)) thus, reducing the surface tension between the system's components allowing more drug to be encapsulated inside the vesicles' hydrophobic milieu (Aburahma and Abdelbary, 2012; Younes et al., 2024). Furthermore, the large alkyl chains of the used SAA (C18 for both) compromised the vesicles' flexibility and improved their stability by preventing their rupture thereby reducing accidental leakage of laded drug (Abdelbary and Fahmy, 2009). Also, it was found that increasing cholesterol percentage might compete with the drug for the accommodating space inside the vesicles, similar findings were obtained by Aboelwafa et al. (2010).

Similarly, Span® 80 contribution (% of total SAA) possessed a positive impact on the %EE ($P = 0.0008$), conveying that increasing its percentage from 30 % to 60 % resulted in higher %EE as shown in Fig. 1B. As mentioned earlier. Span® 80 has a lower HLB value compared to Brij® 92 (4.3 and 5 respectively). Thus, increasing Span® 80 proportion on the expanse of Brij® 92 increased the lipophilicity of the SAA mixture leading to better %EE as previously discussed. Similar results were obtained by Aboelwafa et al. (2010) during the preparation of carvedilol proniosomes where they found that systems based on Brij®72 had lower %EE relative to those based on Span®60.

Table 2
Composition and characterization of TCZ-PNS adopting 2^3 factorial design ($n = 3$, mean ± SD).

Formulae	A: Lecithin: Cholesterol	B: SAA[a]: Cholesterol	C: Span® 80 (% of total SAA)	Y_1: EE[b] (%)	Y_2: Particle size (nm)	Y_3: PDI[c]	Y_4: ZP (mV)
F1	3	1.5	30	71.51 ± 1.24	198.5 ± 3.54	0.25 ± 0.02	−30.71 ± 2.97
F2	3	1.5	60	75.94 ± 3.43	204.2 ± 4.61	0.22 ± 0.04	−30.79 ± 0.42
F3	6	1.5	30	83.15 ± 1.58	225.8 ± 5.09	0.27 ± 0.03	−33.45 ± 1.77
F4	6	1.5	60	86.01 ± 1.62	232.9 ± 0.49	0.23 ± 0.01	−35.35 ± 0.21
F5	3	3	30	73.69 ± 2.49	205.6 ± 3.11	0.24 ± 0.02	−37.31 ± 3.11
F6	3	3	60	78.91 ± 1.24	208.9 ± 2.83	0.21 ± 0.01	−31.55 ± 0.21
F7	6	3	30	84.33 ± 2.84	242.6 ± 3.75	0.24 ± 0.01	−42.65 ± 4.45
F8	6	3	60	89.51 ± 0.94	247.9 ± 0.42	0.23 ± 0.03	−43.42 ± 0.85

SAA[a], Surfactant; EE[b], entrapment efficiency; PDI[c], poly dispersity index; PS[c]; ZP[d], zeta potential.

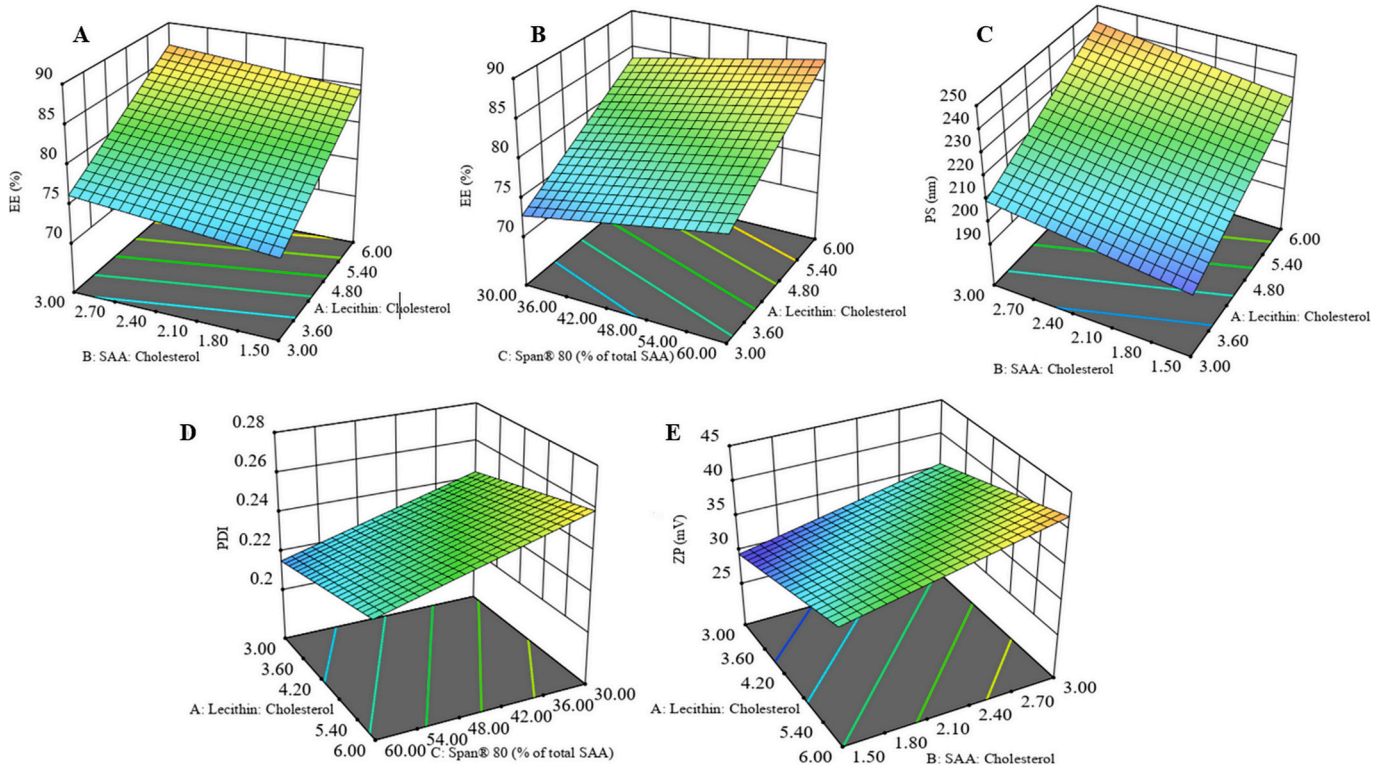

Fig. 1. A: 3D plot showing the effect of lecithin: cholesterol ratio and surfactant: cholesterol ratio on the entrapment efficiency of TCZ-PNS. B: 3D plot showing the effect of lecithin: cholesterol ratio and Span 80® (% of total surfactant) on the entrapment efficiency of TCZ-PNS. C: 3D plot showing the effect of lecithin: cholesterol ratio and surfactant: cholesterol ratio on the particle size of TCZ-PNS. D: 3D plot showing the effect of lecithin: cholesterol ratio and Span 80® (% of total surfactant) on the polydispersity index of TCZ-PNS. E: 3D plot showing the effect of lecithin: cholesterol ratio and surfactant: cholesterol ratio on the zeta potential of TCZ-PNS.

3.1.2. Statistical analysis of particle size (PS) and polydispersity index (PDI)

It is speculated that laded drugs inside nano-sized vesicles could secure better trans-corneal penetration (Dai et al., 2013). Moreover, they should be smaller than 10 μm to avoid ocular irritation Lang et al., 2006. The prepared TCZ-PNS exhibited nanosized vesicles ranging from 198.5 ± 3.54 to 247.9 ± 0.42 nm as summarized in Table 2. ANOVA model analysis declared that only A: Lecithin: Cholesterol and B: SAA: Cholesterol were significantly (P = 0.0002 and 0.0134 respectively) influencing PS as provided in Table 3.

The positive effect of Lecithin: Cholesterol on PS is depicted in Fig. 1C, denoting that increasing the Lecithin's proportion on the expense of Cholesterol would result in greater PS. In the notion of the bulkiness of lecithin's hydrocarbon chain, thus resulting in larger vesicles. C, increasing cholesterol would reduce the bilayer's hydrophilicity prohibiting water intake inside vesicles' core leading to smaller vesicles. These findings coincide with %EE results where higher Lecithin: Cholesterol resulted in higher %EE. Similar results were obtained by Abdelbary et al. (2017) preparing ketoconazole-loaded proniosomal gel.

Likewise, SAA: Cholesterol displayed positive impact on the PS as demonstrated in Fig. 1C, meaning that increasing SAA proportion on behalf of cholesterol produced larger vesicles. Since both SAA used are lipophilic in nature, allowing more drug accommodation in the vesicles' core and causing the expansion of vesicles' bilayer thus, indicating direct correlation between %EE and PS. These results are coinciding those declared by Abdelbary et al. (2017) and Hathout et al. (2007).

The polydispersity index, a ratio of standard deviation to average PS, is an indicator of the vesicles' uniformity as well as the consistency of the preparation technique (Shakeel et al., 2007). A value smaller than 0.5 is recommended to ensure uniform distribution (Clayton et al., 2016). The prepared TCZ-PNS had a PDI value oscillating between 0.21 ± 0.01 and 0.27 ± 0.03 as presented in Table 2. Since all formulae exhibited PDI < 0.5 we could speculate the uniformity of the preparation technique. ANOVA model analysis showed that only A: Lecithin: Cholesterol and C: Span® 80 contribution (% of total SAA) exhibited significant effect on PDI (P = 0.0463 and 0.0063 respectively).

We have found that Lecithin: Cholesterol displayed positive impact on PDI as illustrated in Fig. 1D, which is aligned with PS and %EE results. Since, increasing Lecithin: Cholesterol ratio resulted in larger PS and higher %EE as abovementioned earlier due to the creation of more vesicles for the accommodation of the drug producing larger vesicles of varying sizes which are probably less homogenously distributed (Abdelbari et al., 2021). On the other hand, Span® 80 contribution (% of total SAA) showed a negative impact on PDI as demonstrated in Fig. 1D. Such findings conveyed that increasing Span® 80 resulted in lower PDI and hence more uniformly distributed vesicles. A plausible explanation is the steric hindrance of vesicles coalescence through preferential adsorption of the non-ionic surfactant on vesicles' surface (Ahmed et al., 2022b). Furthermore, Span® 80 would mitigate surface tension through modulating vesicles' curvature thereby stabilizing vesicles' lipid membrane resulting in a unimodal equilateral size distribution pattern (Real et al., 2021).

3.1.3. Statistical analysis of zeta potential (ZP)

The surface charge of vesicles, referred to as zeta potential, plays a pivotal role in impeding particles' flocculation by means of electrostatic repulsion. A higher zeta potential is thus regarded as a general acumen of the system's stability (Ahmed et al., 2022a). According to literature, nanosystems should ideally display a zeta potential, with an absolute value, of at least 30 mV to foster adequate stability (Al-Mahallawi et al., 2015; El Taweel et al., 2023). Regarding the prepared TCZ-PNS, the measured ZP oscillated between −30.71 ± 2.97 mV and − 43.42 ± 0.85 mV as presented in Table 2, so putatively we could expect acceptable stability for all prepared formulae. Statistical analysis and discussion of

ZP results will be in terms of absolute values to provide clear interpretation. ANOVA analysis concluded that only A: Lecithin: Cholesterol and B: SAA: Cholesterol possessed a significant effect ($P = 0.0327$ and 0.0323 respectively) as outlined in Table 3.

Regarding Lecithin: Cholesterol ratio, it had a positive impact on zeta potential as depicted in Fig. 1E, entailing that increasing lecithin proportion augmented zeta potential. Lecithin is a mixture of phospholipids containing phosphate groups which upon hydration tend to ionize providing a negative charge (Eldeeb et al., 2019; Younes et al., 2024). Furthermore, it may alter the hydrophilic milieu surrounding particles by modulating ions and charge distribution thus, consolidating the acquired ZP (Mitrović et al., 2023; Vater et al., 2022).

Similarly, SAA: Cholesterol ratio has positively affected ZP as displayed in Fig. 1E. Despite that Span® 80 and Brij® 92 are non-ionic SAA, a plausible explanation of their contribution to ZP might be that non-ionic SAA preferentially adsorbed at cholesterol/water interface, favored selective adsorption of the negatively charged hydroxyl ions on the expense of positively charged hydronium ion (Exerowa, 1969; Karraker and Radke, 2002). Similar behavior was observed with Tween 80, a non-ionic SAA, which imparted higher negative ZP than anionic SAA like sodium cholate and deoxycholate (El Zaafarany et al., 2010; ElMeshad and Mohsen, 2016)

3.2. Statistical optimization

Integrated desirability algorithms in Design expert® software were utilized to probe independent formulation variables. Eight formulae, generated by the 2^3factorial design, were prepared and characterized followed by imposing restraints on the targeted responses as shown in Table 1. The applied restraints included maximizing %EE and ZP while the PS and PDI were selected to be in range since all systems had acceptable size and homogeneity. An optimum TCZ-PNS was selected based on desirability score (0.91). The composition of the optimum formula was Lecithin: Cholesterol (6:1), SAA: Cholesterol (3:1) and Span® 80 contribution (60 %).

After that, we prepared and characterized the optimum TCZ-PNS followed by calculation of the deviation percentage between measured and software's speculated responses as presented in Table 4. One-way ANOVA analysis was performed, using $\alpha = 0.05$, and declared that the difference between measured and prognosticated responses was not significant validating the optimization process.

Table 4
The actual vs prognosticated responses of the optimum formula and effect of gamma irradiation and short-term stability.*

Response	Y_1	Y_2	Y_3	Y_4
	EE[a] %	PS[b] (nm)	PDI[c]	ZP[d](mV)
Actual value	89.51	247.90	0.23	−43.40
Prognosticated value	89.19	245.40	0.22	−41.66
% Deviation	−0.36	1.02	3.81	4.18

Parameter	Fresh	Gamma irradiation	
		Value	Probability (*p*-value) *
Y_1: EE[a] (%)	89.51 ± 0.94	87.36 ± 2.59	0.384
Y_2: PS[b] (nm)	247.9 ± 0.42	255.50 ± 3.11	0.076
Y_4: ZP[d] (mV)	−43.42 ± 0.85	−45.51 ± 2.55	0.384
Parameter	**Fresh**	**Storage for 3 months at 5 ± 3 °C**	
		Value	**Probability (*p*-value)** *
Y_1: EE[a] (%)	89.51 ± 0.94	87.12 ± 2.45	0.327
Y_2: PS[b] (nm)	247.9 ± 0.42	252.41 ± 2.55	0.133
Y_4: ZP[d] (mV)	−43.42 ± 0.85	−42.75 ± 1.91	0.703

EE[a], entrapment efficiency; PS[b], particle size; PDI[c], poly dispersity index; ZP[d], zeta potential.
* One-way ANOVA statistical analysis.

3.3. Characterization of the optimum TCZ-PNS

3.3.1. Fourier-transform infra-red spectroscopy (FTIR)

The FTIR spectra of TCZ, Cholesterol, Lecithin and the lyophilized optimum TCZ-PNS are depicted in Fig. 2A-D respectively. Regarding TCZ, its FTIR spectrum showed a characteristic peak at 1585 cm^{-1} corresponding to (C = N) stretching, another one at 1465 cm^{-1} representing aromatic (C = C) stretching, an ether (C-O-C) and (C—Cl) stretching bands at 1103 cm^{-1} and 794 cm^{-1} respectively. The FTIR spectrum of Cholesterol showed a hydroxyl stretch band at 3433 cm^{-1}, also a group of peaks (2850–2935 cm^{-1}) corresponding to (CH_2) and (CH_3) asymmetric and symmetric bands (Gupta et al., 2014). Regarding Lecithin, peaks appeared at 2854 cm^{-1} 1739 cm^{-1} and 1234 cm^{-1} were indicative for aliphatic (C—H), carbonyl ester (C=O) and phosphate (P=O) stretch bands respectively (El-Gazayerly et al., 2014). The FTIR spectrum of TCZ-PNS showed that primary peaks of TCZ have disappeared completely as for (C = N), (C-O-C) and (C—Cl) stretching at 1585 cm^{-1},1103 cm^{-1} and 794 cm^{-1} respectively, speculating its accommodation within the optimum system's bilayer (Ahmed et al., 2022a).

3.3.2. Transmission electron microscopy (TEM)

Transmission electron microscopy (TEM) provided better insights into the topological features of prepared nanosytems to consolidate results obtained from dynamic light scattering. As illustrated in Fig. 2E, the micrograph highlighted a flawlessly formed spherical vesicle, with a diameter consistent with the zetasizer's measurements.

3.3.3. Comparative in-vitro release study

As depicted in Fig. 3A, a comparative in-vitro release study has been performed showing the difference between the release pattern of the optimum TCZ-PNS relative to TCZ suspension. The release profile of the optimum TCZ-PNS displayed a bi-phasic release behavior coinciding many proniosomal formulations (Abdelbary et al., 2017; Eldeeb et al., 2019; Sayed et al., 2020; Younes et al., 2024). Such pattern entailed a primary rapid release phase where (≈ 41 %) of drug were released in the first 2 h in contrast to only (≈21 %) for TCZ suspension ($P < 0.05$), preceded by a secondary more sustained phase where (≈88 %) were released compared to only (≈50 %) of drug for TCZ suspension ($P < 0.05$). Moreover, the release profile was subjected to kinetic analysis which determined that Higuchi's diffusion was the best fitting model describing the release behavior ($r^2 = 0.997$, 0.996 for TCZ-PNS and TCZ suspension respectively) (El-Emam et al., 2020; Eldeeb et al., 2019).

Intriguingly, despite that TCZ suspension showed slower release behavior relative to TCZ-PNS, the swift drainage of ophthalmic preparations is demanding sustaining drug release without compromising full drug release to consolidate treatment efficiency while pertaining patient's adherence to dosing schedule.

3.3.4. Corneal ex-vivo permeation study

As illustrated in Fig. 3B, the optimized TCZ-PNS exhibited a statistically significant ($P < 0.05$) improved corneal ex-vivo permeation profile in contrast to TCZ suspension. An important acumen of such improvement is through estimating the cumulative amount permeated of drug at 10 h ($Q_{10h} = 554.39 \pm 15.53$ μg/cm^2 and 302.95 ± 18.02 μg/cm^2 for TCZ-PNS and TCZ suspension respectively). Moreover, the maximum flux (J_{max}) results confirmed such improvement where the optimum TCZ-PNS displayed higher (J_{max}) = 58.59 ± 2.04 μg/cm^2/h relative to TCZ suspension 30.29 ± 1.57 μg/cm^2/h boasting almost doubled permeation performance (ER ≈ 1.8).

The revamped corneal ex-vivo permeation performance of the optimum TCZ-PNS might be attributed to the amalgamation of proniosomal's constituents, nanosized vesicles and negative surface charge. The incorporated SAA (Span® 80 and Brij® 92) contributed in disrupting the tight junction within the epithelium of the cornea (Ahmed et al., 2022a; Younes et al., 2018). Moreover, they are capable of reducing interfacial

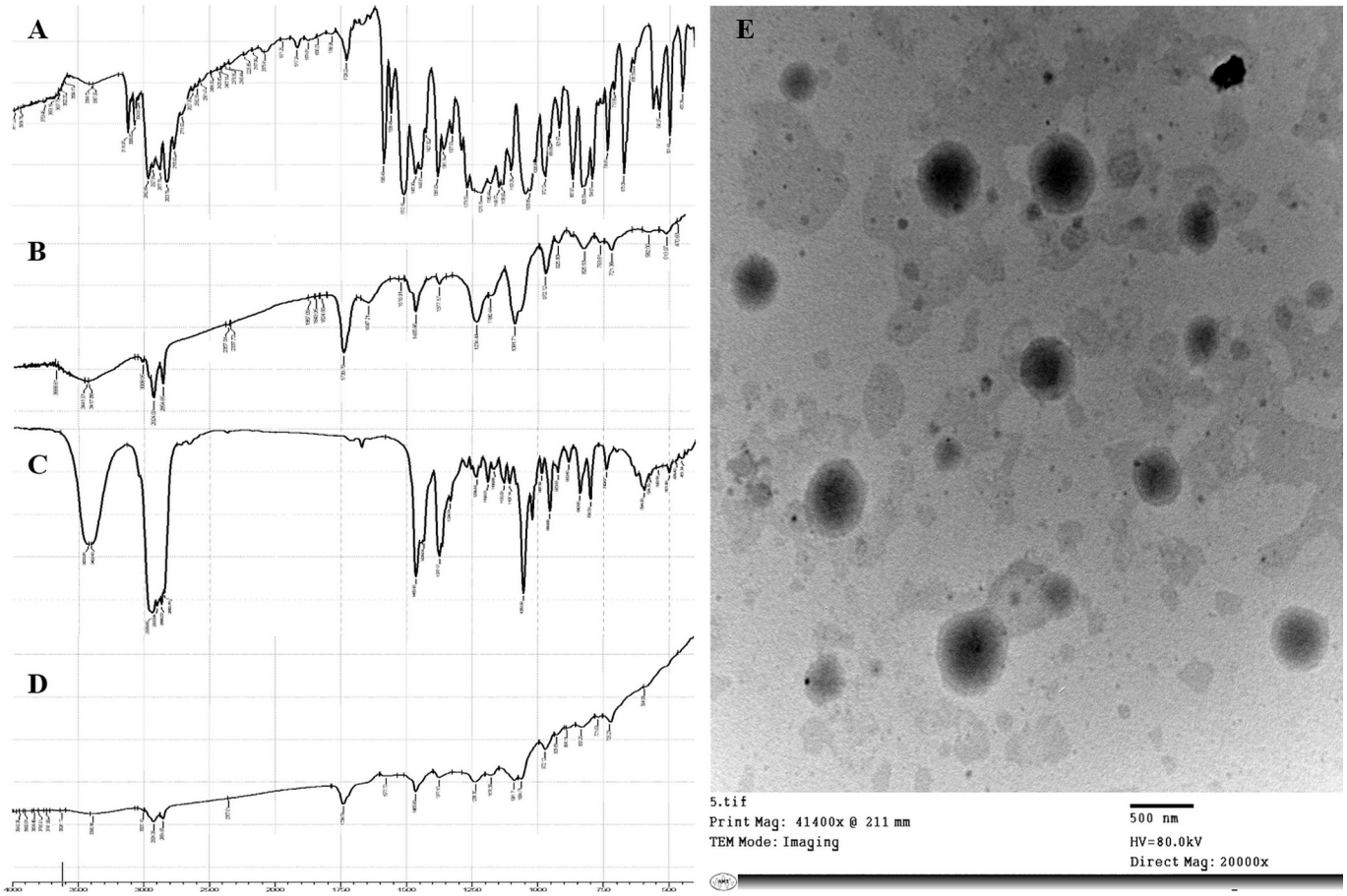

Fig. 2. FTIR spectra of: A: Terconazole (TCZ), B: Lecithin, C: Cholesterol, E: optimized TCZ-PNS. E: Transmission electron micrograph of the reconstituted optimized TCZ-PNS as aqueous niosomal dispersion.

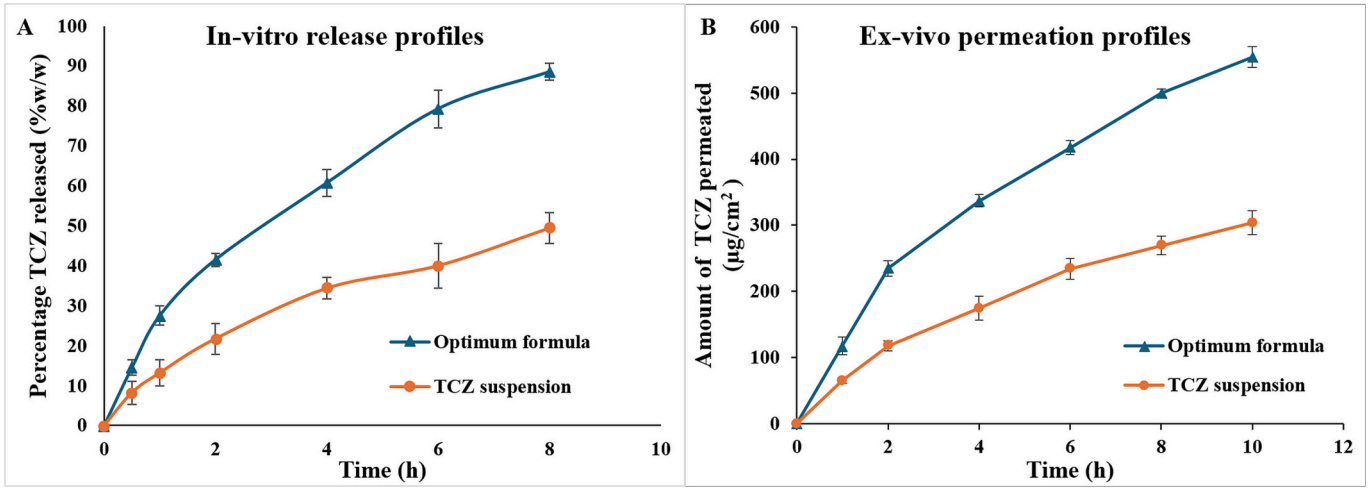

Fig. 3. A: In-vitro release profiles of the optimized TCZ-PNS versus Terconazole suspension in phosphate buffer saline (pH 7.4, 50 mL) containing 10 % methanol (90:10 % *v*/v). B: Corneal ex-vivo permeation profiles of the optimized TCZ-PNS versus Terconazole suspension in simulated tear fluid (pH 7.4, 25 mL).

tension between the corneal membrane and niosomal vesicles. Cholesterol was also reported to act as permeation enhancer thus, improving the diffusion of vesicles through corneal membrane (Eldeeb et al., 2019). Notably, Lecithin played a pivotal role in enhancing drug permeation, being a mixture of phospholipids, it may have modulated lipid bilayer' fluidity, enhanced drug dispersion in physiological fluid through its emulsifying property thereby, enhanced drug contact with physiological membrane (Vater et al., 2019).

Furthermore, better permeation through stroma and prolonged residence time could be an added value for achieving nanosized vesicles (Mosallam et al., 2021). Additionally, the acquired negative surface charge was reported to aid corneal drug penetration through stabilizing the system by keeping the drug loaded nanovesicles in the nanosized range thus facilitating its endocytosis through corneal membrane(Gade

et al., 2019; Gilani et al., 2022). Abdelhakeem et al. (2021) reported that nanostructure lipid carriers loaded with eplerenone and bearing negative charge have revamped permeation in contrast to those bearing positive charges. Similarly, acetazolamide loaded nano-capsules bearing negative charges exhibited enhanced corneal ex-vivo penetration as declared by Quinteros et al. (Quinteros et al., 2016)

3.3.5. Corneal hydration threshold (HT%)

Promptly after the conduction of corneal ex-vivo permeation study, we have measured corneal hydration threshold to investigate possible causality of corneal injury. Naturally, a range of 76–80 % of corneal hydration threshold is considered normal (Huang et al., 2017). Acceptable corneal hydration thresholds were measured for the optimum TCZ-PNS (76.61 % ± 0.28 %) and TCZ suspension (77.97 % ± 1.14 %). One-way ANOVA statistical analysis was performed, and it declared non-significant ($P > 0.05$) difference between TCZ-PNS and TCZ suspension. Therefore, we might conclude that the application of the optimum TCZ-PNS is tolerable (Moustafa et al., 2017).

3.3.6. Effect of short-term storage and Gamma irradiation

A thorough physical examination of the optimum TCZ-PNS following storage and Gamma irradiation which didn't detect any change in the formulation's organoleptic properties or the presence of clumps. The values of %EE, PS and ZP of fresh, stored and Gamma sterilized optimum TCZ-PNS formulae are presented in Table 4. One-way ANOVA analysis concluded that the detected difference between gamma sterilized and stored formula compared to fresh formula regarding %EE, PS and ZP is not significant ($P = 0.384$, 0.076 and 0.384 following Gamma irradiation and 0.327, 0.133 and 0.703 following storage respectively).

Furthermore, the in-vitro release profile of gamma sterilized and stored optimum formula were compared to that of fresh formula using similarity factor ($f2$) and it was found to be 63.6 and 64.45 respectively, declaring that neither storage nor sterilization have affected the release behavior of the optimum formula. Conclusively, the high stability of the optimum TCZ-PNS is attributed to the electrostatic repulsion caused by the acquired high negative ZP (−43.42 ± 0.85 mV) (Harisa and Badran, 2015), stabilizing effect of Lecithin through steric hindrance (Emad Eldeeb et al., 2019) and membrane stabilizing effect owed to Cholesterol's amphiphilic nature thus, impeding vesicles' aggregation (Abdelbari et al., 2021).

3.4. Safety evaluation

3.4.1. Histopathological evaluation

Histopathological evaluation of corneal tissues following instillation of normal saline and optimum TCZ-PNS showed normal epithelium, stroma and endothelium with intact structures and no signs of inflammation as illustrated in Fig. 4A and B respectively. Since instillation of the optimum TCZ-PNS didn't trigger inflammatory responses we could speculate that it has plausible safety profile for ocular application (Abdelbary et al., 2016).

3.4.2. Formulation's pH measurement

Measurement of formulation's pH is an important acumen for the evaluation of safe application of ocular preparations. Since the difference between physiological pH of tear film and that of the optimum TCZ-PNS is very small (7.4 and 7.22 ± 0.13 respectively), therefore the safe application of the optimal formulation could be affirmed (Sayed et al., 2021). Additionally, it was reported that formulation's pH ranging between 4 and 8 might contribute in consolidating better corneal

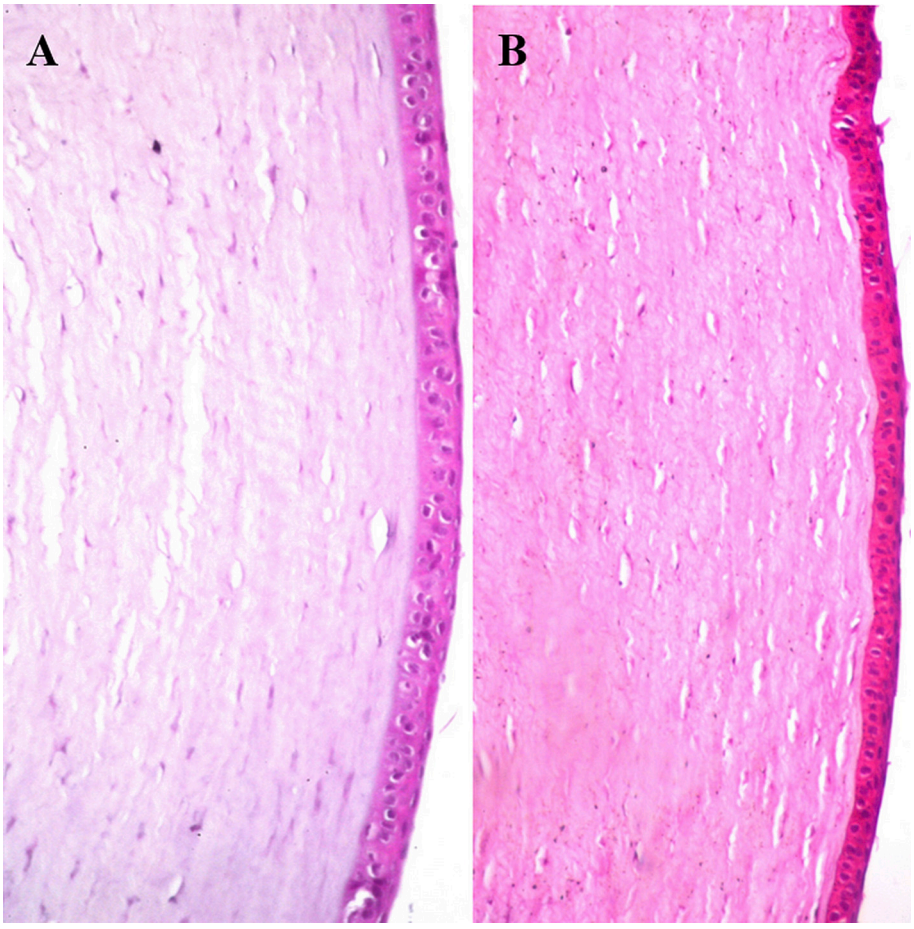

Fig. 4. Histological micrographs of the rabbits' corneas following the instillation of A: Normal saline solution as negative control and B: Optimum TCZ-PNS.

permeation (Mohanty et al., 2013).

3.5. In-vivo permeation and microbiological evaluation

3.5.1. Confocal laser microscopy (CLM)

To prudently evaluate the speculated enhancement of corneal permeation achieved by incorporating TCZ in proniosomal formulation, we have assessed corneal permeation performance of the instilled RhB-PNS vs RhB solution using Confocal Laser Microscopy (CLM). Subsequently, we have recorded detected RhB's emitted fluorescence till reaching maximum depth through corneal tissues. Intriguingly, the optimum RhB-PNS exhibited deeper penetration compared to RhB solution through corneal tissues (60 μm vs 30 μm respectively) following micrographs' analysis as shown in Fig. 5. Such findings coincide with previously discussed corneal ex-vivo permeation results. In the notion of such propitious outcomes, it is prognosticated that TCZ-PNS might be able to deeply deliver antifungal therapy for the eradication of deeply-rooted and inaccessible fungal keratitis (Ahmed et al., 2022a; Younes et al., 2018).

3.5.2. Kirby–Bauer disk diffusion susceptibility test

The optimum TCZ-PNS showed significantly bigger zone of inhibition (29.3 ± 0.76 mm), relative to TCZ suspension zone of inhibition (20.06 ± 0.4 mm) (*t*-test, $P < 0.01$). This finding indicated improvement in antifungal efficacy with the optimized proniosomal formulation.

3.5.3. Minimum inhibitory concentration (MIC)

The minimum inhibitory concentration (MIC) was assessed using the broth microdilution method to confirm the enhancement of the antifungal efficacy indicated by the disk diffusion susceptibility test. The MIC of the optimum TCZ-PNS (0.244 μg/mL) was significantly lower than that of the TCZ suspension (15.625 μg/mL). Statistical significance was assessed by Student's t-test ($P < 0.01$).

3.5.4. Minimum fungicidal concentration (MFC)

Minimum fungicidal concentration (MFC) was determined, for both TCZ suspension and optimum TCZ-PNS, by the broth microdilution technique. Both formulations showed fungicidal effect after 48 h of incubation at 28 °C ± 2. The MFC of the optimum TCZ-PNS (1.95 μg/mL) was significantly lower than that of TCZ suspension (125 μg/mL). The statistics were performed in version 4.1.2 of R (R Core Team, 2022), using Student's t-test ($P < 0.01$). These results confirmed that incorporating TCZ into the optimized PNS significantly enhanced its antifungal activity compared to the TCZ suspension.

3.5.5. Biofilm inhibitory effect of the optimized TCZ-PNS by crystal violet technique

The antibiofilm activity of the optimum TCZ-PNS was compared to that of TCZ suspension against the tested *Candida albicans* ATCC 60193 standard strain by the crystal violet method. The anti-biofilm activity of both formulations was assessed at concentrations of $^1/_8$, $^1/_4$, $^1/_2$, 1, 2, and 4 times the calculated MIC (X), from 0.976 to 0.0305 μg/mL for the optimum formula, and from 62.5 to 1.95312 μg/mL for the TCZ suspension. The optimum TCZ-PNS showed significantly higher biofilm inhibition activity than that of TCZ suspension against the tested *Candida albicans* standard strain (Kruskal-Wallis test, $P < 0.01$) as shown in Fig. 6A.

When paired analysis was applied to test the differences between both preparations for statistical significance at each tested concentration, we found that the biofilm inhibition activity of the optimum TCZ-PNS was significantly higher than that of TCZ suspension against the tested *Candida albicans* standard strain at $^1/_8$, ¼, ½, 1, and 2 X concentrations (Student's t-test, $P < 0.05$) as depicted in Fig. 6B. However, there was no statistical significance between the biofilm inhibition activity of the optimum TCZ-PNS and TCZ suspension at the 4× concentration (Student's t-test, $P = 0.14$) as illustrated in Fig. 6B. These findings suggested that the optimum TCZ-PNS significantly increased the biofilm inhibition activity of TCZ.

4. Conclusion

Terconazole loaded proniosomes were successfully prepared utilizing modified coacervation technique, a 2^3 factorial design was adopted to statistically optimize formulation's independent variables. The optimum TCZ-PNS (desirability = 0.91) boasted plausible %EE (89.51 % ± 0.94 %), nanosized vesicles coinciding TEM measurements (247.9 ± 0.42 nm), sufficiently high zeta potential (−43.42 ± 0.85 mV) and in-vitro bi-phasic release profile which was not affected either by

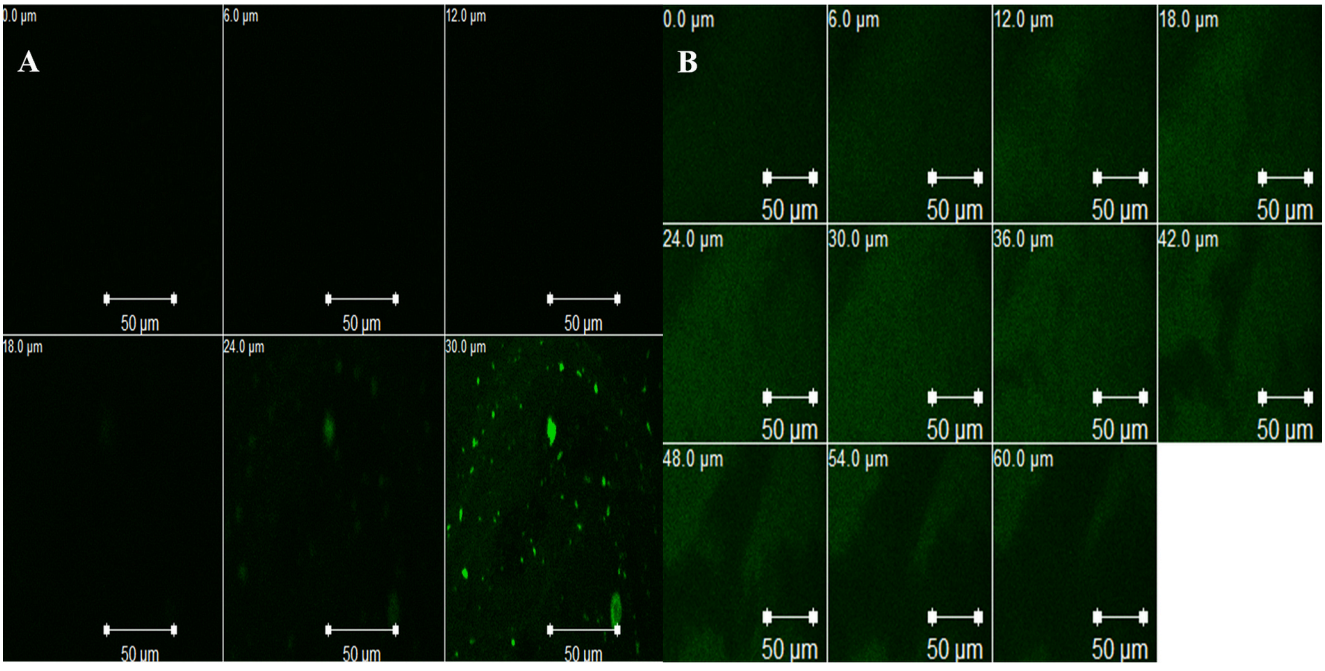

Fig. 5. A: Confocal micrographs of rabbits' corneas following the instillation of RhB-solution and B: RhB-PNS optimized formula.

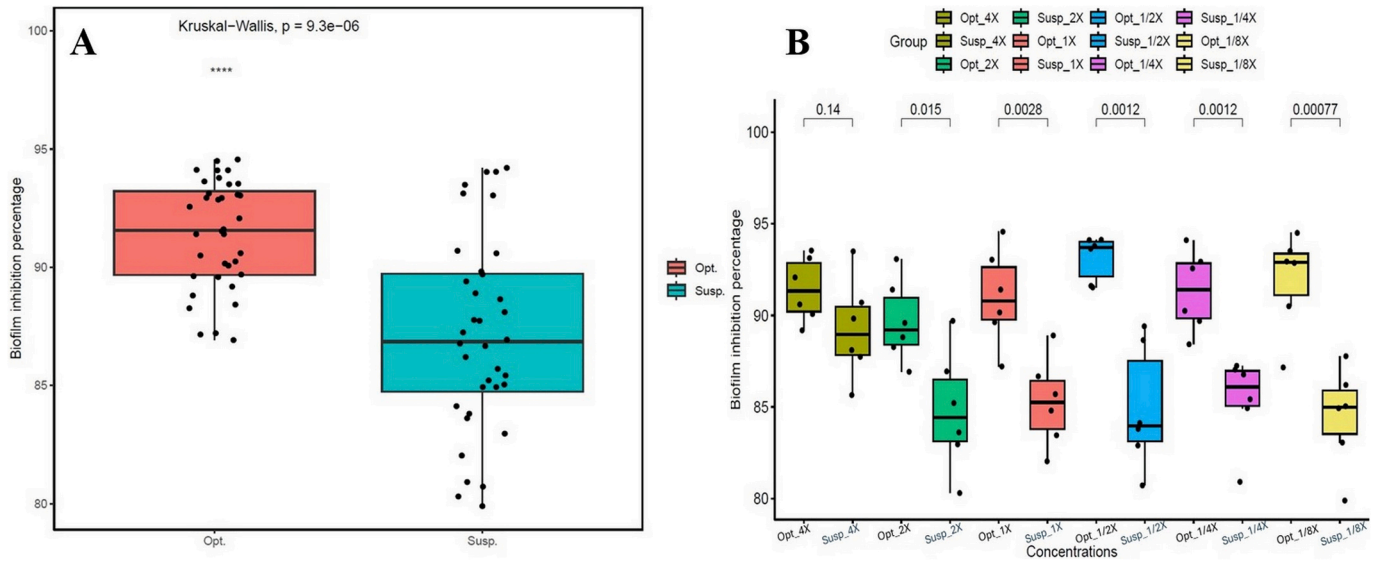

Fig. 6. A: Biofilm inhibition (%) of TCZ suspension (Susp.) and the optimized TCZ-PNS (Opt.). The six tested concentrations are represented by a dot for each replica ($n = 36$). B: Anti-biofilm activity (%) tested at different concentrations against *Candida albicans* standard strain ATCC 60193.

Gamma irradiation or following short-term storage. The corneal ex-vivo permeation of the optimum TCZ-PNS was almost double that of TCZ suspension. The optimum formulation was assessed regarding formulation pH, corneal hydration threshold and histopathological evaluation affirming its safe ocular application.

Confocal laser micrographs illustrated the deep corneal uptake (≈ 2-fold). Moreover, the optimum TCZ-PNS was microbiologically assessed relative to TCZ suspension, and it showed significantly smaller MIC and MFC (64-fold), almost 50 % bigger inhibition zone and most tested concentrations showed higher biofilm inhibition activity. Based on the aforementioned speculations, we could prognosticate that TCZ-PNS might be an auspicious treatment choice to deeply deliver antifungal therapy for the eradication of deeply rooted and inaccessible fungal keratitis.

Ethics approval

All the ex-vivo and in-vivo tests were approved by Research Ethics Committee, Faculty of Pharmacy Cairo University (Approval no. PI 3504) which followed the 507 Guide for Care and Use of Laboratory Animals declared by the US National Institute of Health (NIH 508 Publication No. 85–23, revised 2011).

Consent for publication

Not applicable

CRediT authorship contribution statement

Sadek Ahmed: Writing – review & editing, Supervision, Investigation, Formal analysis, Conceptualization. **Michael M. Farag:** Writing – review & editing, Writing – original draft, Formal analysis. **Heba Attia:** Writing – review & editing, Writing – original draft, Investigation, Formal analysis. **Bander Balkhi:** Supervision, Resources, Conceptualization. **Islam M. Adel:** Supervision, Resources, Investigation. **Asmaa Ashraf Nemr:** Supervision, Resources, Investigation.

Declaration of competing interest

The authors declare that they have no known competing financial interests or personal relationships that could have appeared to influence the work reported in this paper.

Data availability

Data will be made available on request.

Acknowledgement

Researchers Supporting Project number (RSP2025R76), King Saud University, Riyadh, Saudi Arabia.

References

Abdelbari, M.A., El-Mancy, S.S., Elshafeey, A.H., Abdelbary, A.A., 2021. Implementing spanlastics for improving the ocular delivery of clotrimazole: in vitro characterization, ex vivo permeability, microbiological assessment and in vivo safety study. Int. J. Nanomepo09d. 6249–6261.

Abdelbary, A.A., AbouGhaly, M.H., 2015. Design and optimization of topical methotrexate loaded niosomes for enhanced management of psoriasis: application of Box–Behnken design, in-vitro evaluation and in-vivo skin deposition study. Int. J. Pharm. 485, 235–243.

Abdelbary, A.A., Abd-Elsalam, W.H., Al-Mahallawi, A.M., 2016. Fabrication of novel ultradeformable bilosomes for enhanced ocular delivery of terconazole: in vitro characterization, ex vivo permeation and in vivo safety assessment. Int. J. Pharm. 513, 688–696.

Abdelbary, G., Fahmy, R.H., 2009. Diazepam-loaded solid lipid nanoparticles: design and characterization. AAPS Pharm. Sci. Tech. 10, 211–219.

Abdelbary, G.A., Amin, M.M., Zakaria, M.Y., 2017. Ocular ketoconazole-loaded proniosomal gels: formulation, ex vivo corneal permeation and in vivo studies. Drug Deliv. 24, 309–319.

Abdelhakeem, E., El-Nabarawi, M., Shamma, R., 2021. Effective ocular delivery of eplerenone using nanoengineered lipid carriers in rabbit model. Int. J. Nanomed. 4985–5002.

Abdellatif, M.M., Josef, M., El-Nabarawi, M.A., Teaima, M., 2022. Sertaconazole-nitrate-loaded leciplex for treating keratomycosis: optimization using D-optimal design and in vitro, ex vivo, and in vivo studies. Pharmaceutics 14, 2215.

Aboelwafa, A.A., El-Setouhy, D.A., Elmeshad, A.N., 2010. Comparative study on the effects of some polyoxyethylene alkyl ether and sorbitan fatty acid ester surfactants on the performance of transdermal carvedilol proniosomal gel using experimental design. AAPS Pharm. Sci. Tech. 11, 1591–1602.

Aburahma, M.H., Abdelbary, G.A., 2012. Novel diphenyl dimethyl bicarboxylate provesicular powders with enhanced hepatocurative activity: preparation, optimization, in vitro/in vivo evaluation. Int. J. Pharm. 422, 139–150.

Ahmed, S., Amin, M.M., El-Korany, S.M., Sayed, S., 2022a. Corneal targeted fenticonazole nitrate-loaded novasomes for the management of ocular candidiasis: Preparation, in vitro characterization, ex vivo and in vivo assessments. Drug Deliv. 29, 2428–2441.

Ahmed, S., Amin, M.M., El-Korany, S.M., Sayed, S., 2022b. Pronounced capping effect of olaminosomes as nanostructured platforms in ocular candidiasis management. Drug Deliv. 29, 2945–2958.

Ahmed, S., Aziz, D.E., Sadek, M.A., Tawfik, M.A., 2024a. Capped flexosomes for prominent anti-inflammatory activity: development, optimization, and ex vivo and in vivo assessments. Drug Deliv. Transl. Res. 1–14.

Ahmed, S., Farag, M.M., Sadek, M.A., Aziz, D.E., 2024b. Transdermal application of diacerin loaded-terpene enriched invasomes: an approach to augment anti-edema and nociception inhibition activity. J. Liposome Res. 1–14.
Aka, S.T., Haji, S.H., 2015. Sub-MIC of antibiotics induced biofilm formation of Pseudomonas aeruginosa in the presence of chlorhexidine. Braz. J. Microbiol. 46, 149–154.
Al-Badriyeh, D., Leung, L., Davies, G.E., Stewart, K., Kong, D., 2009. Successful use of topical voriconazole 1% alone as first-line antifungal therapy against Candida albicans keratitis. Ann. Pharmacother. 43, 2103–2107.
Al-Badriyeh, D., Neoh, C.F., Stewart, K., Kong, D.C., 2010. Clinical utility of voriconazole eye drops in ophthalmic fungal keratitis. Clin. Ophthalmol. 391–405.
Alhakamy, N.A., Hosny, K.M., Rizg, W.Y., Eshmawi, B.A., Badr, M.Y., Safhi, A.Y., Murshid, S.S., 2022. Development and optimization of hyaluronic acid-poloxamer in-situ gel loaded with voriconazole cubosomes for enhancement of activity against ocular fungal infection. Gels 8, 241.
Al-Mahallawi, A.M., Abdelbary, A.A., Aburahma, M.H., 2015. Investigating the potential of employing bilosomes as a novel vesicular carrier for transdermal delivery of tenoxicam. Int. J. Pharm. 485, 329–340.
Awad, R., Ghaith, A.A., Awad, K., Mamdouh Saad, M., Elmassry, A.A., 2024. Fungal keratitis: diagnosis, management, and recent advances. Clin. Ophthalmol. 85–106.
Bnyan, R., Khan, I., Ehtezazi, T., Saleem, I., Gordon, S., O'Neill, F., Roberts, M., 2018. Surfactant effects on lipid-based vesicles properties. J. Pharm. Sci. 107, 1237–1246.
Bongomin, F., Gago, S., Oladele, R.O., Denning, D.W., 2017. Global and multi-national prevalence of fungal diseases—estimate precision. J. Fungi 3, 57.
Brown, L., Leck, A.K., Gichangi, M., Burton, M.J., Denning, D.W., 2021. The global incidence and diagnosis of fungal keratitis. Lancet Infect. Dis. 21, e49–e57.
Casey-Power, S., Ryan, R., Behl, G., McLoughlin, P., Byrne, M.E., Fitzhenry, L., 2022. Hyaluronic acid: its versatile use in ocular drug delivery with a specific focus on hyaluronic acid-based polyelectrolyte complexes. Pharmaceutics 14, 1479.
Clayton, K.N., Salameh, J.W., Wereley, S.T., Kinzer-Ursem, T.L., 2016. Physical characterization of nanoparticle size and surface modification using particle scattering diffusometry. Biomicrofluidics 10.
CLSI, 2018a. Method for Antifungal Disk Diffusion Susceptibility Testing of Yeasts. Clinical and Laboratory Standards Institute, Wayne, PA.
CLSI, 2018b. Reference Method for Broth Dilution Antifungal Susceptibility Testing of Yeasts; Approved Standard. Clinical and Laboratory Standards Institute, Wayne, PA.
Council N.R., Earth, D.O., Studies, L., Research, I.f.L.A., Care, C.f.t.U.o.t.G.f.t., Animals, U.o.L., 2011. Guide for the Care and Use of Laboratory Animals. National Academies Press.
Dai, Y., Zhou, R., Liu, L., Lu, Y., Qi, J., Wu, W., 2013. Liposomes containing bile salts as novel ocular delivery systems for tacrolimus (FK506): in vitro characterization and improved corneal permeation. Int. J. Nanomed. 1921–1933.
Davies, N.M., 2000. Biopharmaceutical considerations in topical ocular drug delivery. Clin. Exp. Pharmacol. Physiol. 27, 558–562.
Ding, D., Kundukad, B., Somasundar, A., Vijayan, S., Khan, S.A., Doyle, P.S., 2018. Design of mucoadhesive PLGA microparticles for ocular drug delivery. ACS Appl. Bio Mater. 1, 561–571.
El Taweel, M.M., Tawfik, M.A., Soliman, K., Khattab, M.S., Farag, M.M., 2023. Tailoring of topically applied curcumin loaded pro-novasomes for skin cancer treatment: In-vitro characterization, statistical optimization and histopathological assessment of subcutaneous Ehrlich carcinoma mice model. J. Drug Deliv. Sci. Technol. 88, 104957.
El Zaafarany, G.M., Awad, G.A., Holayel, S.M., Mortada, N.D., 2010. Role of edge activators and surface charge in developing ultradeformable vesicles with enhanced skin delivery. Int. J. Pharm. 397, 164–172.
Eldeeb, A.E., Salah, S., Ghorab, M., 2019. Formulation and evaluation of cubosomes drug delivery system for treatment of glaucoma: Ex-vivo permeation and in-vivo pharmacodynamic study. J. Drug Deliv. Sci. Technol. 52, 236–247.
El-Emam, G.A., Girgis, G.N., El-Sokkary, M.M.A., El-Azeem Soliman, O.A., Abd El Gawad, A.E.G.H., 2020. Ocular inserts of voriconazole-loaded proniosomal gels: formulation, evaluation and microbiological studies. Int. J. Nanomed. 7825–7840.
El-Gazayerly, O., Makhlouf, A., Soelm, A., Mohmoud, M., 2014. Antioxidant and hepatoprotective effects of silymarin phytosomes compared to milk thistle extract in CCl4 induced hepatotoxicity in rats. J. Microencapsul. 31, 23–30.
ElMeshad, A.N., Mohsen, A.M., 2016. Enhanced corneal permeation and antimycotic activity of itraconazole against Candida albicans via a novel nanosystem vesicle. Drug Deliv. 23, 2115–2123.
Emad Eldeeb, A., Salah, S., Ghorab, M., 2019. Proniosomal gel-derived niosomes: an approach to sustain and improve the ocular delivery of brimonidine tartrate; formulation, in-vitro characterization, and in-vivo pharmacodynamic study. Drug Deliv. 26, 509–521.
Exerowa, D., 1969. Effect of adsorption, ionic strength and p H on the potential of the diffuse electric layer. Kolloid-Zeitschrift und Zeitschrift für Polymere 232, 703–710.
Farag, M.M., Louis, M.M., Badawy, A.A., Nessem, D.I., Elmalak, N.S.A., 2022. Drotaverine hydrochloride superporous hydrogel hybrid system: a gastroretentive approach for sustained drug delivery and enhanced viscoelasticity. AAPS PharmSciTech 23, 124.
Farag, M.M., El-Nassan, H.B., Merey, H.A., Eltanany, B.M., Galal, M.M., Wadie, W., El-Tanbouly, D.M., Khattab, M.A., Rashed, L.A., ElMeshad, A.N., 2023a. Comparative pharmacodynamic study delineating the efficacy of amantadine loaded nano-emulsified organogel via intranasal versus transdermal route in rotenone-induced Parkinson's disease rat model. J. Drug Deliv. Sci. Technol. 86, 104765.
Farag, M.M., El-Sebaie, W., Basalious, E.B., El-Gazayerly, O.N., 2023b. Darifenacin self-assembled liquid crystal cubic nanoparticles: a sustained release approach for an overnight control of overactive bladder. AAPS Pharm. Sci. Tech. 24, 120.
Gade, S., Patel, K.K., Gupta, C., Anjum, M.M., Deepika, D., Agrawal, A.K., Singh, S., 2019. An ex vivo evaluation of moxifloxacin nanostructured lipid carrier enriched in situ gel for transcorneal permeation on goat cornea. J. Pharm. Sci. 108, 2905–2916.
Gaudana, R., Ananthula, H.K., Parenky, A., Mitra, A.K., 2010. Ocular drug delivery. AAPS J. 12, 348–360.
Gavarkar, P.S., Adnaik, R.S., Mohite, S.K., 2013. An overview of azole antifungals. Int. J. Pharm. Sci. Res. 4, 4083.
Gilani, S.J., Jumah, M.N.B., Zafar, A., Imam, S.S., Yasir, M., Khalid, M., Alshehri, S., Ghuneim, M.M., Albohairy, F.M., 2022. Formulation and evaluation of nano lipid carrier-based ocular gel system: optimization to antibacterial activity. Gels 8, 255.
Gupta, U., Singh, V.K., Kumar, V., Khajuria, Y., 2014. Spectroscopic studies of cholesterol: fourier transform infra-red and vibrational frequency analysis. Mater. Focus 3, 211–217.
Habib, B.A., Sayed, S., Elsayed, G.M., 2018. Enhanced transdermal delivery of ondansetron using nanovesicular systems: fabrication, characterization, optimization and ex-vivo permeation study-Box-Cox transformation practical example. Eur. J. Pharm. Sci. 115, 352–361.
Haney, E.F., Trimble, M.J., Hancock, R.E.W., 2021. Microtiter plate assays to assess antibiofilm activity against bacteria. Nat. Protoc. 16, 2615–2632.
Harisa, G.I., Badran, M.M., 2015. Simvastatin nanolipid carriers decreased hypercholesterolemia induced cholesterol inclusion and phosphatidylserine exposure on human erythrocytes. J. Mol. Liq. 208, 202–210.
Hathout, R.M., Mansour, S., Mortada, N.D., Guinedi, A.S., 2007. Liposomes as an ocular delivery system for acetazolamide: in vitro and in vivo studies. AAPS PharmSciTech 8, E1–E12.
Huang, J., Peng, T., Li, Y., Zhan, Z., Zeng, Y., Huang, Y., Pan, X., Wu, C.-Y., Wu, C., 2017. Ocular cubosome drug delivery system for timolol maleate: preparation, characterization, cytotoxicity, ex vivo, and in vivo evaluation. AAPS PharmSciTech 18, 2919–2926.
Ismail, S., Khattab, A., 2018. Optimization of proniosomal itraconazole formulation using Box Behken design to enhance oral bioavailability. J. Drug Deliv. Sci. Technol. 45, 142–150.
Karraker, K., Radke, C., 2002. Disjoining pressures, zeta potentials and surface tensions of aqueous non-ionic surfactant/electrolyte solutions: theory and comparison to experiment. Adv. Colloid Interface Sci. 96, 231–264.
Kondawar, M., Kamble, K., Malusare, M., Waghmare, J., Shah, N., 2011. Proniosome based drug delivery system for clotrimazole. Res. J. Pharmacy Technol. 4, 1284–1287.
Kouchak, M., Mahmoodzadeh, M., Farrahi, F., 2019. Designing of a pH-triggered Carbopol®/HPMC in situ gel for ocular delivery of dorzolamide HCl: in vitro, in vivo, and ex vivo evaluation. AAPS PharmSciTech 20, 1–8.
Lang, J.C., Roehrs, R.E., Jani, R., 2006. Ophthalmic preparations. Remington 1, 850–854.
Leck, A., Thomas, P., Hagan, M., Kaliamurthy, J., Ackuaku, E., John, M., Newman, M., Codjoe, F., Opintan, J., Kalavathy, C., 2002. Aetiology of suppurative corneal ulcers in Ghana and South India, and epidemiology of fungal keratitis. Br. J. Ophthalmol. 86, 1211–1215.
Liu, Z., Pan, W., Nie, S., Zhang, L., Yang, X., Li, J., 2005. Preparation and evaluation of sustained ophthalmic gel of enoxacin. Drug Dev. Ind. Pharm. 31, 969–975.
Mahajan, S.S., Chaudhari, R., Patil, V., 2021. Formulation and evaluation of topical proniosomal gel of ciclopirox for antifungal therapy. Int. J. Pharm. Invest. 11.
Mahale, N., Thakkar, P., Mali, R., Walunj, D., Chaudhari, S., 2012. Niosomes: novel sustained release nonionic stable vesicular systems—an overview. Adv. Colloid Interface Sci. 183, 46–54.
Mannermaa, E., Vellonen, K.-S., Urtti, A., 2006. Drug transport in corneal epithelium and blood–retina barrier: emerging role of transporters in ocular pharmacokinetics. Adv. Drug Deliv. Rev. 58, 1136–1163.
Mirza, R., Ahirrao, S., Kshirsagar, S., 2017. A nanocrystal technology: to enhance solubility of poorly water soluble drugs. J. Appl. Pharm. Res. 5, 01–13.
Mitrović, J.R., Divović-Matović, B., Knutson, D.E., Petković, M., Djorović, D., Randjelović, D.V., Dobričić, V.D., Đoković, J.B., Lunter, D.J., Cook, J.M., 2023. High amount of lecithin facilitates oral delivery of a poorly soluble pyrazoloquinolinone ligand formulated in lipid nanoparticles: Physicochemical, structural and pharmacokinetic performances. Int. J. Pharm. 633, 122613.
Mohanty, B., Mishra, S.K., Majumdar, D.K., 2013. Effect of formulation factors on in vitro transcorneal permeation of voriconazole from aqueous drops. J. Adv. Pharm. Technol. Res. 4, 210–216.
Mohsen, A.M., 2022. Cationic polymeric nanoparticles for improved ocular delivery and antimycotic activity of terconazole. J. Pharm. Sci. 111, 458–468.
Mosallam, S., Ragaie, M.H., Moftah, N.H., Elshafeey, A.H., Abdelbary, A.A., 2021. Use of novasomes as a vesicular carrier for improving the topical delivery of terconazole: in vitro characterization, in vivo assessment and exploratory clinical experimentation. Int. J. Nanomed. 119–132.
Mosallam, S., Albash, R., Abdelbari, M.A., 2022. Advanced vesicular systems for antifungal drug delivery. AAPS PharmSciTech 23, 206.
Moustafa, M.A., Elnaggar, Y.S., El-Refaie, W.M., Abdallah, O.Y., 2017. Hyalugel-integrated liposomes as a novel ocular nanosized delivery system of fluconazole with promising prolonged effect. Int. J. Pharm. 534, 14–24.
Nemr, A.A., El-Mahrouk, G.M., Badie, H.A., 2021. Development and evaluation of proniosomes to enhance the transdermal delivery of cilostazole and to ensure the safety of its application. Drug Dev. Ind. Pharm. 47, 403–415.
Nemr, A.A., El-Mahrouk, G.M., Badie, H.A., 2022. Development and evaluation of surfactant-based elastic vesicular system for transdermal delivery of Cilostazole: ex-vivo permeation and histopathological evaluation studies. J. Liposome Res. 32, 159–171.

Nemr, A.A., Ahmed, S., Adel, I.M., 2024. Limonene-enriched ultra-structural cubosomes to augment ocular delivery of a poorly water soluble anti-fungal drug: fabrication, characterization, statistical optimization, in vivo corneal uptake and histopathological evaluation in rabbits. J. Drug Deliv. Sci. Technol. 105886.
O'Toole, G.A., 2011. Microtiter dish biofilm formation assay. J. Vis. Exp. 47, 2437.
Qiao, G.L., Ling, J., Wong, T., Yeung, S.N., Iovieno, A., 2020. Candida keratitis: epidemiology, management, and clinical outcomes. Cornea 39, 801–805.
Quinteros, D.A., Ferreira, L.M., Schaffazick, S.R., Palma, S.D., Allemandi, D.A., Cruz, L., 2016. Novel polymeric nanoparticles intended for ophthalmic administration of acetazolamide. J. Pharm. Sci. 105, 3183–3190.
R Core Team, 2022. R: A Language and Environment for Statistical Computing. R Foundation for Statistical Computing, Vienna, Austria.
Real, D.A., Hoffmann, S., Leonardi, D., Goycoolea, F.M., Salomon, C.J., 2021. A quality by design approach for optimization of Lecithin/Span® 80 based nanoemulsions loaded with hydrophobic drugs. J. Mol. Liq. 321, 114743.
Sayed, S., Abdelmoteleb, M., Amin, M.M., Khowessah, O.M., 2020. Effect of formulation variables and gamma sterilization on transcorneal permeation and stability of proniosomal gels as ocular platforms for antiglaucomal drug. AAPS PharmSciTech 21, 1–13.
Sayed, S., Abdel-Moteleb, M., Amin, M.M., Khowessah, O.M., 2021. Cubogel as potential platform for glaucoma management. Drug Deliv. 28, 293–305.
Shahab, M.S., Rizwanullah, M., Alshehri, S., Imam, S.S., 2020. Optimization to development of chitosan decorated polycaprolactone nanoparticles for improved ocular delivery of dorzolamide: in vitro, ex vivo and toxicity assessments. Int. J. Biol. Macromol. 163, 2392–2404.
Shakeel, F., Baboota, S., Ahuja, A., Ali, J., Aqil, M., Shafiq, S., 2007. Nanoemulsions as vehicles for transdermal delivery of aceclofenac. AAPS PharmSciTech 8, 191–199.
Sharma, N., Bagga, B., Singhal, D., Nagpal, R., Kate, A., Saluja, G., Maharana, P.K., 2022. Fungal keratitis: a review of clinical presentations, treatment strategies and outcomes. Ocul. Surf. 24, 22–30.
Tawfik, M.A., Eltaweel, M.M., Farag, M.M., Shamsel-Din, H.A., Ibrahim, A.B., 2023. Sonophoresis-assisted transdermal delivery of antimigraine-loaded nanolipomers: Radio-tracking, histopathological assessment and in-vivo biodistribution study. Int. J. Pharm. 644, 123338.
Taymouri, S., Varshosaz, J., 2016. Effect of different types of surfactants on the physical properties and stability of carvedilol nano-niosomes. Adv. Biomed. Res. 5, 48.
Vater, C., Adamovic, A., Ruttensteiner, L., Steiner, K., Tajpara, P., Klang, V., Elbe-Bürger, A., Wirth, M., Valenta, C., 2019. Cytotoxicity of lecithin-based nanoemulsions on human skin cells and ex vivo skin permeation: Comparison to conventional surfactant types. Int. J. Pharm. 566, 383–390.
Vater, C., Bosch, L., Mitter, A., Göls, T., Seiser, S., Heiss, E., Elbe-Bürger, A., Wirth, M., Valenta, C., Klang, V., 2022. Lecithin-based nanoemulsions of traditional herbal wound healing agents and their effect on human skin cells. Eur. J. Pharm. Biopharm. 170, 1–9.
Weng, J., Tong, H.H., Chow, S.F., 2020. In vitro release study of the polymeric drug nanoparticles: development and validation of a novel method. Pharmaceutics 12, 732.
Whitcher, J.P., Srinivasan, M., Upadhyay, M.P., 2001. Corneal blindness: a global perspective. Bull. World Health Organ. 79, 214–221.
Younes, N.F., Abdel-Halim, S.A., Elassasy, A.I., 2018. Corneal targeted Sertaconazole nitrate loaded cubosomes: preparation, statistical optimization, in vitro characterization, ex vivo permeation and in vivo studies. Int. J. Pharm. 553, 386–397.
Younes, N.F., Sayed, S., Hassan, M., Ahmed, S., 2024. Engineered lecithin-based proniosomes for enhanced trans-tympanic permeation: in vitro, microbiological, ex vivo and in vivo evaluation. J. Drug Deliv. Sci. Technol. 96, 105728.
Yousry, C., Zikry, P.M., Salem, H.M., Basalious, E.B., El-Gazayerly, O.N., 2020. Integrated nanovesicular/self-nanoemulsifying system (INV/SNES) for enhanced dual ocular drug delivery: statistical optimization, in vitro and in vivo evaluation. Drug Deliv. Transl. Res. 10, 801–814.
Zaghloul, N., El Hoffy, N.M., Mahmoud, A.A., Elkasabgy, N.A., 2022a. Cyclodextrin stabilized freeze-dried silica/chitosan nanoparticles for improved terconazole ocular bioavailability. Pharmaceutics 14, 470.
Zaghloul, N., Mahmoud, A.A., Elkasabgy, N.A., El Hoffy, N.M., 2022b. PLGA-modified Syloid®-based microparticles for the ocular delivery of terconazole: in-vitro and in-vivo investigations. Drug Deliv. 29, 2117–2129.